

Diffusion reaction of oxygen in aluminum oxide films on silicon

E. B. O. da Rosa,* I. J. R. Baumvol, J. Morais, and R. M. C. de Almeida
Instituto de Física, UFRGS, Av. Bento Gonçalves 9500, Porto Alegre, RS 91509-900, Brazil

R. M. Papaléo
Faculdade de Física, PUCRS, Av. Ipiranga 6681, C.P. 1429, Porto Alegre, RS 90619-900, Brazil

F. C. Stedile
Instituto de Química, UFRGS, Av. Bento Gonçalves 9500, Porto Alegre, RS 91509-900, Brazil

(Received 8 October 2001; published 11 March 2002)

Aluminum oxide films deposited on silicon by atomic layer chemical vapor deposition were annealed in an ^{18}O -enriched oxygen atmosphere under various conditions of temperature, time, and pressure. Cavity formation at the film surface was monitored by atomic force microscopy and it was seen to depend on annealing parameters. Areal densities and profiles of oxygen incorporated from the gas phase were determined by nuclear reaction techniques. A propagating front of incorporated oxygen from the gas/solid interface toward the film/substrate interface was observed. This was modeled as a diffusion-reaction process, where isotopic exchange is the reaction channel. The model is capable of reproducing the observed ^{18}O profiles and areal densities as well as their dependence on annealing parameters.

DOI: 10.1103/PhysRevB.65.121303

PACS number(s): 66.30.Pa, 24.30.-v, 68.37.Ps

Gate dielectric film thinning is required by the progress in the integration level of silicon-based metal-oxide-semiconductor field-effect transistors (MOSFET). Current commercial devices incorporate silicon oxynitride gate dielectrics as thin as 2 nm or less, forcing the dielectric to operate under extreme conditions, compromising device performance and reliability.¹ Replacing the SiO_2 -based dielectric by a material of higher dielectric constant (high- k material) can, in principle, solve this problem^{1,2} and a promising candidate is aluminum oxide.^{3,1} For a critical evaluation of its suitability, it is imperative to know how Al_2O_3 films deposited on Si behave upon thermal annealing in oxygen-containing atmospheres. Previous investigations^{1,4,5} demonstrated that a post-deposition annealing in O_2 reduces leakage current and density of electronic states at the high- k material/Si interface down to acceptable limits. On the other hand, studies on ultrathin Al_2O_3 films on Si (Refs. 6–8) showed that thermal annealing in O_2 can also lead to undesirable consequences: oxidation of the Si substrate giving rise to a SiO_2 layer, which creates a gate dielectric stack whose overall dielectric constant is lower than that of Al_2O_3 ,¹ and Si migration from the substrate into the Al_2O_3 films.⁷ Annealing temperature is also a controversial parameter since high temperatures induce film crystallization, creating preferential diffusion paths, but on the other hand increase the material k , decrease the amount of contaminants present in the as-deposited film,⁹ and anneal dopants. Thus, it is necessary to find annealing conditions that result in optimum electrical properties. This is apparently obtained by allowing mobile oxygen to reach the Al_2O_3 /Si interface in amounts that, while contributing to reduce interface trap density and leakage current, do not substantially oxidize the Si substrate. Indeed two questions remain: how deep can oxygen go in the films as a function of annealing parameters and what is the transport mechanism in these films? This is the object of the present work.

Starting samples were 35 nm thick amorphous Al_2O_3 films deposited by atomic layer chemical vapor deposition (ALCVD) (Ref. 10) on Si(001) substrates. The choice of such relatively thick films (as compared to what would be useful in actual MOS devices) aims at keeping the Al_2O_3 /Si interface well apart from the surface, allowing a better understanding of atomic transport phenomena. These samples were submitted to rapid thermal annealings (RTA) in dry-oxygen enriched to 98.5% in the ^{18}O isotope ($^{18}\text{O}_2$). Annealing in $^{18}\text{O}_2$ together with nuclide-specific analysis permits distinction between oxygen eventually incorporated during thermal treatment and oxygen originally in the films, given that the natural abundance of ^{18}O is only 0.2%. ^{18}O profiles (concentration versus depth curves) were obtained by narrow nuclear reaction resonance profiling (NRP) with a depth resolution of approximately 0.8 nm in the near-surface region of the films and by SPACES simulations.^{11–13} Areal densities of incorporated ^{18}O were determined by nuclear reaction analysis (NRA).¹¹ Atomic force microscopy (AFM) images were collected on a Digital Instruments Nanoscope IIIa in tapping mode.

The surface of the as-deposited sample is smooth, with a root-mean-square roughness of about 0.2 nm. Thermal annealing in 6 mbar of $^{18}\text{O}_2$ for 300 s does not produce any significant change in the film surface up to temperatures around 750 °C as shown in Fig. 1(a), which is very similar to the image of the as-deposited sample. Nevertheless, after annealing at 800 °C the surface presents holes 30–50 nm in diameter and 2–5 nm deep [Fig. 1(b)]. If the exposure time is increased to 720 s, the onset of hole formation occurs at lower temperatures and a distribution similar to the one in Fig. 1(b) is already seen at 750 °C [Fig. 1(d)]. The onset temperature and time for hole formation are also decreased when higher $^{18}\text{O}_2$ pressures are used [Figs. 1(e) and 1(f)]. These holes are deeper (5–8 nm) and seem to coalesce yielding wider cavities. Moreover, hole distribution is not as

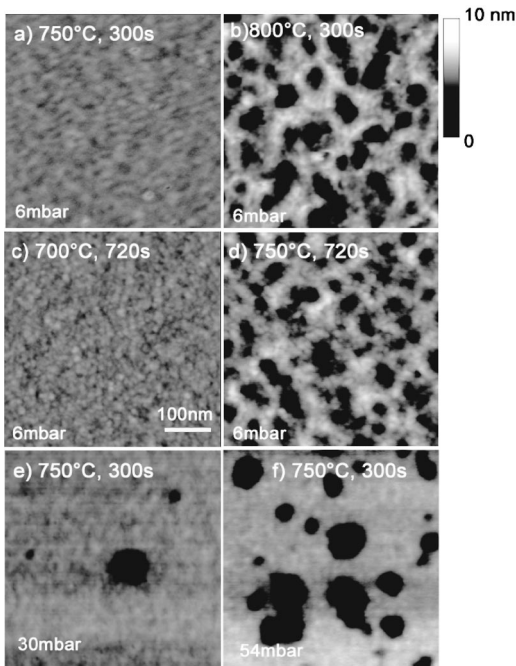


FIG. 1. TM-AFM images of Al_2O_3 films on Si after thermal treatments in $^{18}\text{O}_2$ at different annealing conditions.

densely packed and regular as the one seen at lower pressure and higher temperature [Fig. 1(b)] or higher exposure time [Fig. 1(d)]. Thus, the onset of cavity formation, its areal density, and spatial distribution are shown to be functions of oxygen pressure, temperature, and time of annealing, and can be controlled by a careful choice of these parameters. Based on these findings, a model to explain cavity formation should include the role of oxygen in this process. Investigation of this question both theoretically and experimentally is intended in the near future.

^{18}O profiles as determined by NRP in samples annealed for different times are shown in Fig. 2(a). The areas under the excitation curves were normalized by the areal densities of ^{18}O incorporated in the films, independently determined by NRA. The amount and range of ^{18}O incorporated in the films increase with time of annealing. In the case of the sample annealed for 720 s a substantial amount of oxygen is incorporated near the $\text{Al}_2\text{O}_3/\text{Si}$ interface while the AFM image of this sample [Fig. 1(d)] evidences the formation of cavities. NRP results obtained with annealings at increasing temperatures are shown in Fig. 2(b). It can be seen that more oxygen is incorporated into the films at higher annealing temperatures.

The results of NRP also indicate that the mechanism of oxygen diffusion and incorporation in Al_2O_3 films on Si is different from that in SiO_2 films on Si.^{11,14} Indeed, when 20 nm thick SiO_2 films are annealed in $^{18}\text{O}_2$, minor amounts of ^{18}O are fixed in the near-surface region^{14,15} while most of the ^{18}O is incorporated near the SiO_2/Si interface^{11,16} with no interaction and consequently no incorporation of ^{18}O in the bulk of the films. In the present case, as evidenced by profiles in Fig. 2, oxygen from the gas phase diffuses in the film strongly interacting with the Al_2O_3 network being thus incorporated in near-surface and bulk regions. This incorpora-

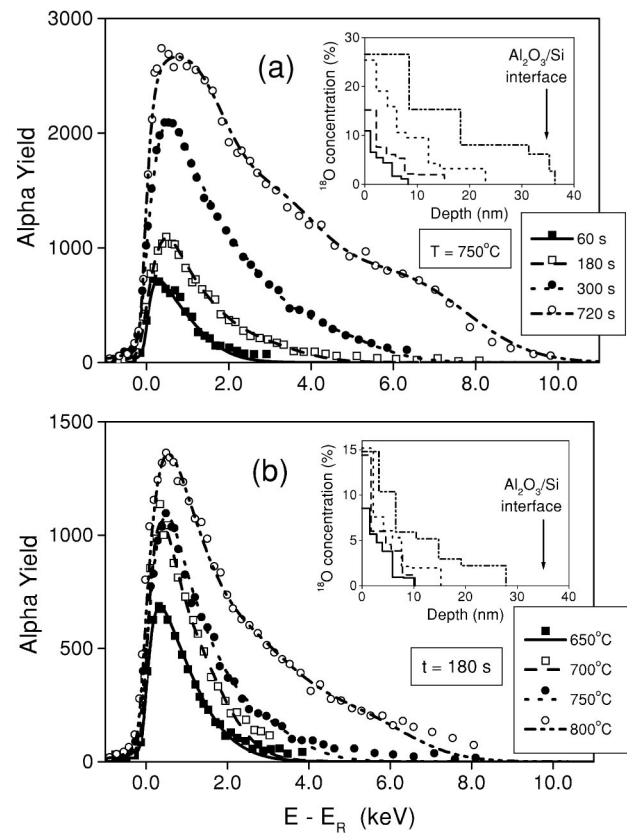


FIG. 2. Experimental excitation curves (symbols) for the $^{18}\text{O}(p,\alpha)^{15}\text{N}$ nuclear reaction around the 151 keV resonance and the corresponding simulations (lines) for Al_2O_3 films on Si after annealing under 6 mbar of $^{18}\text{O}_2$: at 750 °C for different times (a) and for 180 s for different temperatures (b). ^{18}O profiles assumed in the simulations are shown in the insets.

tion of ^{18}O in Al_2O_3 films could take place by means of exchange with O atoms originally in the films⁷ and/or by net incorporation (changing the oxide stoichiometry). Recent studies⁹ on oxidation in $^{18}\text{O}_2$ of 45 nm thick Al_2O_3 films demonstrated that ^{18}O incorporation is almost entirely due to the ^{16}O - ^{18}O exchange. Furthermore, these studies also pointed out that the ^{16}O - ^{18}O exchange process may be bridged by OH or H species which exist in Al_2O_3 films as a consequence of the deposition process (ALCVD) and of exposure to air. N_2 annealing of these films prior to oxidation led to a decrease in the amount of incorporated H and ^{18}O evidencing the effect of densification. On the other hand, oxidation in $^{18}\text{O}_2$ of much thinner (3-6 nm) Al_2O_3 films on Si (Refs. 6 and 7) showed that reaction with Si at the interface is a parallel channel of ^{18}O incorporation. The present findings evidence that this last channel is only activated when the propagating front of diffusive ^{18}O reaches the interface.

These experimental findings can be modeled as a diffusion-reaction process,^{7,17} considering an initial thick layer of Al_2O_3 exposed to $^{18}\text{O}_2$ that starts diffusing in the Al_2O_3 network. We modeled ^{16}O and ^{18}O in two different states: diffusive (*d*) and fixed (*f*). The diffusive state represents mobile, nonincorporated oxygen, that exists only when

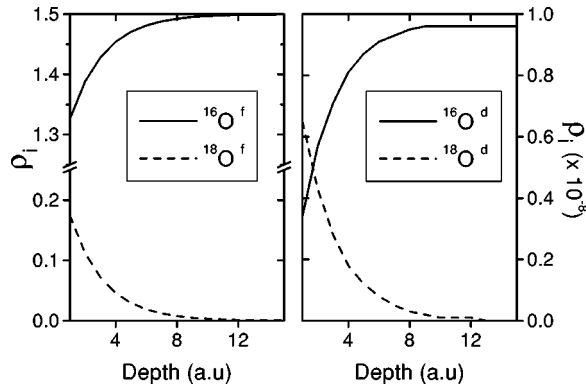


FIG. 3. Typical calculated profiles of fixed and diffusive ^{16}O and ^{18}O in Al_2O_3 films. The profile of $^{16}\text{O}^d$, after reaching a maximum, decreases towards greater depths (tail not shown). The amount of $^{16}\text{O}^d$ (obtained by integrating the area under the curve) is of the order of the amount of $^{18}\text{O}^f$.

the film is under annealing conditions ($^{18}\text{O}_2$ -pressure and high temperature). Diffusive ^{18}O may displace fixed ^{16}O with probability k , fixing ^{18}O in the network and generating diffusive ^{16}O . The reversal reaction is also possible. Local densities of these species are described by their relative atomic concentrations $\rho_i(x,t) = C_i(x,t)/C_{\text{Al}}^{\text{Al}_2\text{O}_3}$, where C_i is the concentration of the i th species (^{16}O or ^{18}O , d or f) and $C_{\text{Al}}^{\text{Al}_2\text{O}_3}$ is the concentration of Al atoms in Al_2O_3 ; x measures the depth from the surface and t the elapsed time, implying a mean field approximation over the directions parallel to the surface. Before RTA the species densities are $\rho_{^{16}\text{O}^d}(x,0) = \rho_{^{18}\text{O}^d}(x,0) = \rho_{^{16}\text{O}^f}(x,0) = 0, \rho_{^{18}\text{O}^f}(x,0) = 1.5$. The time evolution of the density functions is described by the following differential equations:

$$\begin{aligned} \frac{\partial \rho_{^{16}\text{O}^d}}{\partial t} &= D \frac{\partial^2 \rho_{^{16}\text{O}^d}}{\partial x^2} + k[\rho_{^{18}\text{O}^d} \rho_{^{16}\text{O}^f} - \rho_{^{16}\text{O}^d} \rho_{^{18}\text{O}^f}], \\ \frac{\partial \rho_{^{18}\text{O}^d}}{\partial t} &= D \frac{\partial^2 \rho_{^{18}\text{O}^d}}{\partial x^2} - k[\rho_{^{18}\text{O}^d} \rho_{^{16}\text{O}^f} - \rho_{^{16}\text{O}^d} \rho_{^{18}\text{O}^f}], \\ \frac{\partial \rho_{^{16}\text{O}^f}}{\partial t} &= -\frac{\partial \rho_{^{18}\text{O}^f}}{\partial t} = -k[\rho_{^{18}\text{O}^d} \rho_{^{16}\text{O}^f} - \rho_{^{16}\text{O}^d} \rho_{^{18}\text{O}^f}], \end{aligned} \quad (1)$$

where D and k are the diffusivity of oxygen in Al_2O_3 and the rate of oxygen isotopic exchange reaction, respectively. Boundary condition is given by $\rho_{^{18}\text{O}^d}(0,t) = p_{\text{O}}$, where p_{O} is the concentration of diffusive ^{18}O at the Al_2O_3 film surface. The solution for the sum of the diffusive species is direct: $\rho_{^{18}\text{O}^d} + \rho_{^{16}\text{O}^d} = p_{\text{O}} \text{erfc}(x/2\sqrt{Dt})$. For the other species, Eqs. (1) are numerically iterated. Typical calculated density function profiles are shown in Fig. 3. They reproduce the trend of experimental results (see Fig. 2), namely a decreasing incorporated ^{18}O profile from the surface into the bulk of the Al_2O_3 film.

The dependence of the areal densities of incorporated ^{18}O on the $^{18}\text{O}_2$ pressure was also experimentally determined and the result is presented in Fig. 4(a). A linear dependence

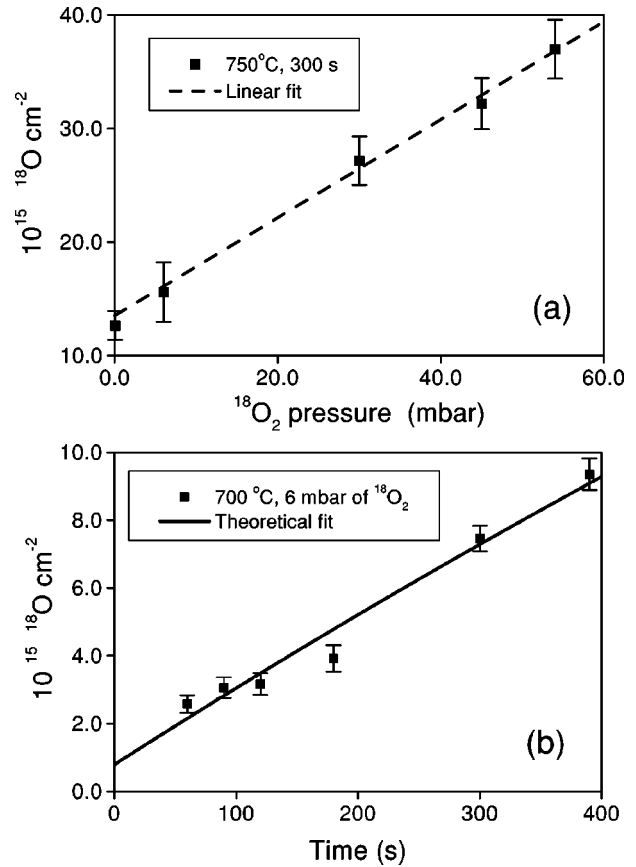


FIG. 4. (a) Areal densities of ^{18}O incorporated in the films after annealing under pressures between 0.06 and 54 mbar. The dashed line is from a linear fit to the data; (b) kinetics of oxygen incorporated in the films. The solid curve represents the theoretical result. Error bars account for measurement uncertainties.

on the $^{18}\text{O}_2$ pressure is observed in the pressure range studied in this work, differently from that observed in the case of SiO_2 films on Si, where the ^{18}O areal density in the near-surface region follows a $p_{\text{O}}^{1/4}$ law.¹⁴ However, this information alone does not allow us to specify the kind of network defect associated with oxygen isotopic exchange in $\text{Al}_2\text{O}_3/\text{Si}$ structures. Note that the relatively shallow cavities observed by AFM have little influence on the uptake of ^{18}O in 35 nm thick films. However, cavities may become decisive for the incorporation of oxygen when the Al_2O_3 film thickness is comparable to the hole depth. Previous results⁷ obtained with 6.5 nm Al_2O_3 films on Si were attributed⁸ to thickness inhomogeneities of the films, although no AFM image of the sample surface was provided at that moment. The present results prove the proposed interpretation.

Various combinations of annealing conditions involving moderate pressures, temperatures, and times guarantee amounts of ^{18}O incorporated much smaller than those of remaining ^{16}O . In this case the reaction terms in Eqs. (1) may be linearized, that is $\rho_{^{18}\text{O}^f} \ll \rho_{^{16}\text{O}^f} \sim 1.5$ and then $k[\rho_{^{18}\text{O}^d} \rho_{^{16}\text{O}^f} - \rho_{^{16}\text{O}^d} \rho_{^{18}\text{O}^f}] \sim 1.5k\rho_{^{18}\text{O}^d}$. This approximation simply states that the incorporation of ^{18}O depends on its concentration and reaction rate only, since it is diffusing in a

“sea” of fixed ^{16}O . The model becomes then analytically soluble and the amount of ^{18}O incorporated in the network is given by

$$\chi(t) = \chi_0 + 2p_O \sqrt{\frac{D}{1.5k}} \left[\frac{\sqrt{1.5kt} e^{-1.5kt}}{2\sqrt{\pi}} + \frac{3kt-1}{4} \operatorname{erf}(\sqrt{1.5kt}) \right] \quad (2)$$

where $\chi_0 = \chi(t=0)$. The calculated amount of ^{18}O incorporated is thus directly proportional to p_O in accordance with the present experimental observation and it is clear from the above expression that curves of $(\chi - \chi_0)/(p_O \sqrt{D/1.5k})$ versus kt will all collapse into the same curve,¹⁷ allowing the fitting of experimental kinetics as shown in Fig. 4(b). To obtain values for D and k one must estimate p_O . For a rough, first estimate one can take the p_O value used for SiO_2 at O_2 pressures around 6 mbar,¹⁸ which is around 10^{-8} . The fit then yields values for D and k of the order of $10^6 \text{ nm}^2/\text{s}$ and 10^5 s^{-1} , respectively. One must recall here that Fig. 4(b) represents only that portion of the calculated kinetics corresponding to the time range of experimental points. In fact, one can infer from Eq. (2) that the model kinetics is not linear. Values of D and k extracted from the fitting were used to calculate profiles of incorporated ^{18}O , yielding results

compatible with those experimentally determined. However, reliable determinations of D and k require further work aiming at first principles estimates of diffusive oxygen adsorbed at the film surface^{15,19} as well as kinetics curves covering wider time intervals.

In summary, during annealing in dry-oxygen of Al_2O_3 films on Si, oxygen is transported by a mechanism whereby mobile oxygen atoms or molecules from the gas phase are exchanged for O atoms fixed in the Al_2O_3 network. The films, whose surfaces are initially very smooth, may present cavities after thermal treatment. However, surface smoothness can be tailored by choosing adequate annealing parameters. A propagating front of oxygen incorporated from the surface toward the interface was experimentally observed. This was modeled by diffusion-reaction equations, capable of reproducing the observed amounts and profiles of oxygen incorporated as well as their dependence on annealing parameters. For practical purposes of future Si-based MOSFET devices it is essential to control the propagation of the diffusive oxygen front. This requires detailed kinetics experiments, accurate values of surface concentration of adsorbed oxygen as a function of oxidation parameters, as well as the diffusivity and reaction rate of oxygen in Al_2O_3 films on Si, which will render the model quantitative.

Work was partially supported by CNPq, PADCT, and FAPERGS.

*Electronic address: erosa@if.ufrgs.br

¹G.D. Wilk, R.M. Wallace, and J.M. Anthony, *J. Appl. Phys.* **89**, 5243 (2001), and references therein.

²A.I. Kingon, J.P. Maria, and S.K. Streiffer, *Nature (London)* **406**, 1032 (2000).

³E.P. Gusev, M. Copel, E. Cartier, I.J.R. Baumvol, C. Krug, and M.A. Gribelyuk, *Appl. Phys. Lett.* **76**, 176 (2000).

⁴D. Landheer, J.A. Gupta, G.I. Sproule, J.P. McCaffrey, M.J. Graham, K.C. Yang, Z.H. Lu, and W.N. Lennard, *J. Electrochem. Soc.* **148**, G29 (2001).

⁵B.H. Lee, L. Kang, R. Nieh, W.J. Qi, and J.C. Lee, *Appl. Phys. Lett.* **76**, 1926 (2000).

⁶M. Copel, E. Cartier, E.P. Gusev, S. Guha, N. Bojarczuk, and M. Poppeller, *Appl. Phys. Lett.* **78**, 2670 (2001).

⁷C. Krug, E.B.O. da Rosa, R.M.C. de Almeida, J. Morais, I.J.R. Baumvol, T.D.M. Salgado, and F.C. Stedile, *Phys. Rev. Lett.* **85**, 4120 (2000).

⁸M. Copel, *Phys. Rev. Lett.* **86**, 4713 (2001).

⁹L.G. Gosset *et al.*, in *Proceedings of the International Workshop on Device Technology*, edited by I.J.R. Baumvol and J. Morais

(Materials Research Society, Porto Alegre, 2001).

¹⁰T. Suntola, *Appl. Surf. Sci.* **100/101**, 391 (1996).

¹¹I.J.R. Baumvol, *Surf. Sci. Rep.* **36**, 1 (1999), and references therein.

¹²G. Battistig, G. Amsel, I. Trimaille, J.J. Ganem, S. Rigo, F.C. Stedile, I.J.R. Baumvol, W.H. Schulte, and H.W. Becker, *Nucl. Instrum. Methods Phys. Res. B* **85**, 326 (1994).

¹³I. Vickridge and G. Amsel, *Nucl. Instrum. Methods Phys. Res. B* **45**, 6 (1990).

¹⁴I. Trimaille and S. Rigo, *Appl. Surf. Sci.* **39**, 65 (1989).

¹⁵D.R. Hamann, *Phys. Rev. Lett.* **81**, 3447 (1998).

¹⁶F. Rochet, B. Agius, and S. Rigo, *J. Electrochem. Soc.* **131**, 914 (1984).

¹⁷R.M.C. de Almeida, S. Gonçalves, I.J.R. Baumvol, and F.C. Stedile, *Phys. Rev. B* **61**, 12 992 (2000).

¹⁸S. Rigo, in *The Physics and Chemistry of SiO_2 and the Si-SiO₂ Interface*, edited by C. R. Helms and B. E. Deal (Plenum Publishing, New York, 1988), p. 75.

¹⁹J.R. Chelikowsky, D.J. Chadi, and N. Binggeli, *Phys. Rev. B* **62**, R2251 (2000).